Hindawi Publishing Corporation
ISRN Condensed Matter Physics
Volume 2013, Article ID 646042, 9 pages
http://dx.doi.org/10.1155/2013/646042

Research Article

Ab Initio Investigation of Nitride in Comparison with Carbide Phase of Superconducting Ti_2InX (X = C, N)

M. Roknuzzaman and A. K. M. A. Islam

Department of Physics, Rajshahi University, Rajshahi 6205, Bangladesh

Correspondence should be addressed to A. K. M. A. Islam; azi46@ru.ac.bd

Received 30 October 2012; Accepted 11 December 2012

Academic Editors: M. Durandurdu, A. Krimmel, and A. D. Zaikin

The structural, elastic, electronic, thermal, and optical properties of superconducting nanolaminates Ti_2InX (X = C, N) are investigated by density functional theory (DFT). The results obtained from the least studied nitride phase are discussed in comparison with those of carbide phase having T_c value half as that of the former. The carbide phase is found to be brittle in nature, while the nitride phase is less brittle. Elastic anisotropy demonstrates that the c-axis is stiffer in Ti_2InN than in Ti_2InC. The band structure and density of states show that these phases are conductors, with contribution predominantly from the Ti 3d states. The bulk modulus, Debye temperature, specific heats, and thermal expansion coefficient are obtained as a function of temperature and pressure for the first time through the quasiharmonic Debye model with phononic effects. The estimated values of electron-phonon coupling constants imply that Ti_2InC and Ti_2InN are moderately coupled superconductors. The calculated thermal expansion coefficient is in fair agreement with the only available measured value for Ti_2InC. Further the first time calculated optical functions reveal that the reflectivity is high in the IR-visible-UV region up to ~10 eV and 12.8 eV for Ti_2InC and Ti_2InN, respectively, showing these to be promising coating materials.

1. Introduction

The so-called nanolaminates (or MAX) phases since their discovery by Nowotny [1] have attracted a lot of interest among the research community due to their remarkable properties having attributes of both ceramic and metal [2–24]. Ceramic attributes include lightweight, elastically rigid, and high temperatures strength, whereas metallic attributes show the phases to be thermally and electrically conductive, quasiductile, and damage tolerant. Currently there are about 60 synthesized MAX phases [3]. Out of these only seven low-T_c superconductors have so far been identified. These are Mo_2GaC [4], Nb_2SC [5], Nb_2SnC [6], Nb_2AsC [7], Ti_2InC [8], Nb_2InC [9], and Ti_2InN [10].

The X-ray diffraction, magnetic, and resistivity measurements discovered that Ti_2InX (X = C, N) are superconductors [8, 10] with superconducting temperatures of 3.1 and 7.3 K, respectively. In fact Bortolozo et al. [10] in 2010 showed unambiguously that Ti_2InN is the first nitride superconductor belonging to the $M_{n+1}AX_n$ family. Among the ternary phases almost all the studies are concerned with carbide properties, but a very limited work on nitrides which was discovered in 1963 by Jeitschko et al. [12]. This nitride crystallizes in the same prototype structure as carbides (Cr_2AlC), where the basic structural component is an octahedron of six Ti atoms with an N atom instead of C [16]. It has also been shown that the interactions in the Ti_6N octahedra are stronger than those in TiN octahedra in agreement with the general trend known for binary carbides and nitrides [16]. Further calculations show that the nitride phase has higher density of states at Fermi level than that of carbide phase. All these point to the role of N atom in changing the electronic structure and the possible transport properties which were the motivation of Bortolozo et al. [10] to seek superconductivity in nitride phase. These motivate us to revisit the system Ti_2InX (X = C, N) and investigate further the influence of the substitution of N for C on the M_2AX nanolaminates.

Some works on elastic and electronic structures of Ti_2InC have been carried out by several groups of workers [15–20,

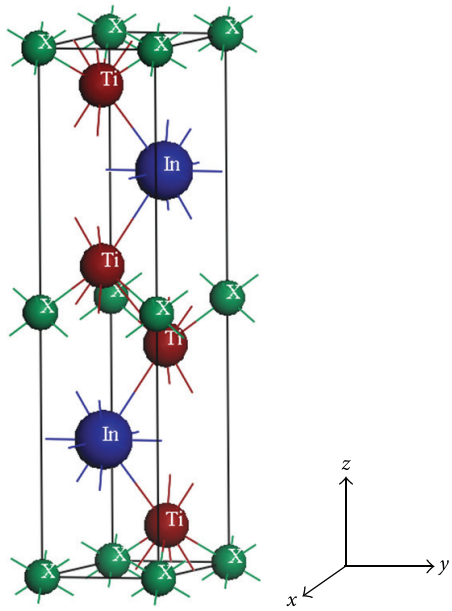

Figure 1: Crystal structure of layered MAX phases Ti_2InX (X = C, N).

22, 23] using several different methodologies. A theoretical study of the elastic properties for six of the seven known superconducting MAX phases: Nb_2SC, Nb_2SnC, Nb_2AsC, Nb_2InC, Mo_2GaC, and Ti_2InC has been presented by Shein and Ivanovskii [20]. Long before this Ivanovskii et al. [16] calculated the electronic structure of the H-phases Ti_2MC and Ti_2MN (M = Al, Ga, In) by the self-consistent linearized muffin-tin-orbital method in the atomic-sphere approximation and the MO LCAO method using RMH parameterization. The band structure and bonding configuration of the H-phases are compared with those of other Ti-M-C and Ti-M-N phases. The energy band structure of the Ti_2InC along with some other MAX phases has been calculated in the framework of the full-potential augmented-plane-wave method under GGA [17]. Medkour et al. [18] reported on the electronic properties of only M_2InC phases by employing the pseudo potential plane wave (PP-PW) method using CASTEP. He et al. [19] have performed *ab initio* calculations for the structural, elastic, and electronic properties of only M_2InC. Benayad et al. [22] very recently included Ti_2InN along with Ti_2InC to investigate the structural, elastic, and electronic properties by using the full-potential linear muffin-tin orbital (FP-LMTO) method. The exchange and correlation potential is treated by the local density approximation (LDA).

Despite all the above efforts, it is clear that T_2InN has been subjected to limited study. Moreover full optical as well as finite-temperature and finite-pressure thermodynamical studies are absent for both the superconducting phases. Therefore there is a need to highlight those areas where little or no work has been carried out. We are thus inclined to address these areas of the two nanolaminates as well as revisit the existing theoretical works so as to provide elastic, electronic properties of the nitride phase in comparison with carbide phase. The optical properties such as dielectric function, absorption spectrum, conductivity, energy-loss spectrum and reflectivity for both the phases will be calculated and discussed.

2. Computational Techniques

The *ab initio* calculations were performed using the plane-wave pseudopotential method within the framework of the density functional theory [25] implemented in the CASTEP code [26]. The ultrasoft pseudopotentials were used in the calculations, and the plane-wave cutoff energy was 500 eV. The exchange-correlation terms used are of the Perdew-Berke-Ernzerhof form of the generalized gradient approximation [27]. We have used a $10 \times 10 \times 2$ Monkhorst-pack [28] grid to sample the Brillouin zone. All the structures were relaxed by BFGS methods [29]. Geometry optimization was performed using convergence thresholds of 1×10^{-5} eV/atom for the total energy, 0.03 eV/Å for the maximum force, 0.05 GPa for maximum stress, and 1×10^{-3} Å for the maximum displacements. The elastic constants C_{ij}, bulk modulus B, and electronic properties were directly calculated by the CASTEP code.

The quasiharmonic Debye model [30] has been employed to investigate the finite-temperature and finite-pressure thermodynamic properties. Here the thermodynamic parameters can be calculated at any temperature and pressure using the DFT calculated E-V data at $T = 0$ K, $P = 0$ GPa, and the Birch-Murnaghan third order EOS [31].

3. Results and Discussion

3.1. Structural and Elastic Properties. The superconducting MAX phases Ti_2InC and Ti_2InN possess the hexagonal structure with space group $P6_3/mmc$ (no. 194) as shown in Figure 1. The unit cell contains two formula units, and the atoms occupy the following Wyckoff positions: the Ti atoms in the position $4f[(1/3, 2/3, z_M), (2/3, 1/3, z_M + 1/2), (2/3, 1/3, -z_M), (1/3, 2/3, -z_M + 1/2)]$, the In atoms in the position $2d$ $\{(1/3, 2/3, 3/4), (2/3, 1/3, 1/4)]$, and the C atoms (or, N atoms) in the position $2a[(0, 0, 0), (0, 0, 1/2)]$, where z_M is the internal parameter [2, 32].

The calculated fully relaxed equilibrium values of the structural parameters of the two superconducting phases are presented in Table 1 together with other available data on both theoretical [15, 19, 20, 22, 23] and experimental [11, 13, 14] results . The comparison shows that the calculated values are in good agreement with the available experimental as well as theoretical results.

The elastic constant tensors of the superconducting MAX phases Ti_2InC and Ti_2InN are reported in Table 2 along with available computed elastic constants [15, 20, 22, 23]. For Ti_2InC the agreement with available theoretical results is quite good. But for Ti_2InN, the only set of data due to Benayad et al. [22] deviate much from our calculations and also from the trend for similar phase (Table 2). The reason may be the use of FP-LMTO method treated with LDA with P-W parameterization.

Table 1: Calculated lattice parameters (a and c in Å), ratio c/a and internal parameters z_M for the superconducting MAX phases Ti_2InC and Ti_2InN.

Phase	a	c	c/a	z_M	Reference
Ti_2InC	3.1453	14.215	4.519	0.0780	Present
	3.1373	14.1812	4.520	0.0783	[15]
	3.14	14.17	4.51	0.0779	[19]
	3.1485	14.2071	4.512	0.0780	[20]
	3.084	13.906	4.508	0.0788	[22]
	3.135	14.182	4.524		[23]
	3.134	14.077	4.492		[11] Experimental data
	3.133	14.10	4.5		[14] Experimental data
Ti_2InN	3.0956	14.063	4.543	0.07855	Present
	3.033	13.727	4.525	0.07908	[22]
	3.07	13.97	4.54		[13] Experimental data

Table 2: Calculated elastic constants (C_{ij}, in GPa), bulk moduli (B, in GPa), shear moduli (G, in GPa), Young's moduli (Y, in GPa), Poisson's ratio (ν), A and k_c/k_a for superconducting Ti_2InC and Ti_2InN.

Phase	C_{11}	C_{12}	C_{13}	C_{33}	C_{44}	B	G	Y	ν	A	k_c/k_a	Reference
Ti_2InC	284.2	58.7	52.3	246.1	90.0	126.4	100.4	240	0.184	0.798	1.230	Present
	273.4	62.9	50.3	232.3	87.2	120	96	228	0.184	0.829	1.293	[15]
	282.6	70.2	54.9	232.9	57.6	124.7	81.7	201.1	0.232	0.542	1.365	[20]
	281.0	57.7	44.5	226.6	85.8		98.6			0.768	1.371	[22]
	287.0	65	53	244	85	128	99			0.766	1.288	[23]
Ti_2InN	213.7	36.8	105.6	231.7	98	125.5	81	200	0.234	1.11	0.312	Present
	102.9	60.9	62.7	106.1	46.1	41.8[a]	32.9	86.3	0.31	2.19	0.884	[22]

[a] Calculated based on data from [22].

Using the second-order elastic constants, the bulk modulus B, shear modulus G (all in GPa), Young's modulus Y, and Poisson's ratio ν at zero pressure are calculated and presented in Table 2. The pressure dependence of the elastic constants is a very important characterization of the crystals with varying pressure and/or temperature, but we defer it till in a later section. The ductility of a material can be roughly estimated by the ability of performing shear deformation, such as the value of shear-modulus-to-bulk-modulus ratios. Thus a ductile plastic solid would show low G/B ratio (<0.5); otherwise, the material is brittle. As is evident from Table 2, the calculated G/B ratios are 0.8 and 0.65 for carbide and nitride phases, respectively, indicating that first compound is brittle in nature and the second one will be more on the brittle/ductile border line. The same can be inferred from an additional argument that the variation in the brittle/ductile behavior follows from the calculated Poisson's ratio. For brittle material the value is small enough, whereas for ductile metallic materials ν is typically 0.33 [24].

The elastic anisotropy of the shear of hexagonal crystals, defined by $A = 2C_{44}/(C_{11} - C_{12})$, may be responsible for the development of microcracks in the material [36]. This factor is unity for an ideally isotropic crystal. The calculated value of A increases from 0.798 to 1.11 as C atom is replaced by N. We can also examine a second anisotropy parameter which is the ratio between the uniaxial compression values along the c- and a-axis for a hexagonal crystal: $k_c/k_a = (C_{11} + C_{12} - 2C_{13})/(C_{33} - C_{13})$. We find that the compressibility of Ti_2InC along the c-axis is larger than along the a-axis ($k_c/k_a = 1.23$) in agreement with other calculations [15, 20, 22, 23], but for Ti_2InN the situation is reversed, as c is stiffer for this material.

3.2. Electronic Bonding Properties. The energy bands of the two nanolaminates along the high symmetry directions in the first Brillouin zone are shown in Figures 2(a) and 2(b) in the energy range from −15 to +5 eV. The band structures of both the superconducting phases reveal 2D-like behaviour with smaller energy dispersion along the c-axis and in the K-H and L-M directions. The 2D behaviour does not differ much from one superconductor to the other, except that the bands of the nitride phase are shifted more towards the Fermi level. The occupied valence bands of Ti_2InC and Ti_2InN lie in the energy range from −8.8 eV to Fermi level and −9.5 eV to Fermi level, respectively. Further, the valence and conduction bands are seen to overlap, thus indicating metallic-like behaviour of both the phases. This conductivity increases as C is replaced by N. The In 4d and C 2s-type quasicore bands with a small dispersion can be seen in the energy intervals ~ −13.7 to −14.4 eV and from −11 to −10 eV, respectively below the Fermi level. The corresponding energy intervals are about −14 to −15 eV for In 4d and N 2s-type quasicore bands. As seen in [15] the multiband character of the systems can be inferred from three near Fermi bands which intersect the Fermi level.

The total and partial densities of states for the two superconducting phases are illustrated in Figures 3(a) and

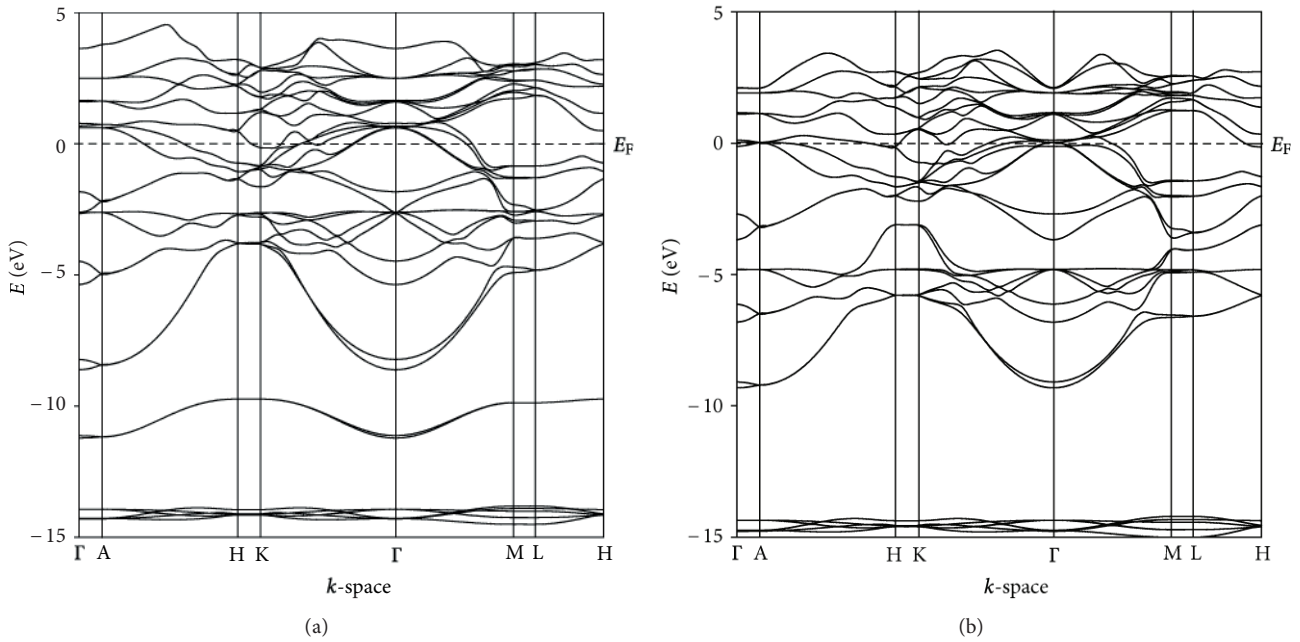

Figure 2: Calculated band structures of (a) Ti_2InC and (b) Ti_2InN.

3(b). The values of DOS at the Fermi level are 2.78 and 4.98 states/eV which predominantly contain contributions from the Ti 3*d* states of 2.22 and 4.06 states/eV of the two phases Ti_2InC and Ti_2InN, respectively. The diffuse character of both *s* and *p* states of In atoms causes larger dispersion of In bands than those due to C and N. A covalent interaction occurs (−9 eV to Fermi level) between the constituting elements as a result of the degeneracy of the states with respect to both angular momentum and lattice site. C *p*, N *p*, and Ti *d* as well as In *p* and Ti *d* states are all hybridized. Such hybridization peak of Ti *d*–C *p* in Ti_2InC and Ti *d*–N *p* in Ti_2InN lies lower in energy (−5 to −2 eV) and (−7 to −4 eV) than that of Ti *d*–In *p* (−3 eV to Fermi level). All these indicate that Ti–In bond is weaker than either Ti–C or Ti–N bond. The population analysis shows that bond lengths in Å for Ti_2InC and Ti_2InN in increasing order are as Ti–C (2.1277), Ti–Ti (2.8661), Ti–In (3.0456), In–C (3.9908) and Ti–N (2.1010), Ti–Ti (2.8416), Ti–In (3.0013), and In–N (3.9439). The bands associated with N atoms are narrower and lower in energy. This is attributed to the large electronegativity of N compared to that of C.

Ivanovskii et al. [16] from their band structure calculations for the phases suggest that the transition metal does not play role in the superconducting mechanism suggesting that the transport behaviour of this material is of 2D nature. The C atom is less electronegative than N, and the chemical bond between Ti–C is less polarized than Ti–N. It is thus hypothesized [16] that the electrons of the basal plane rather than the *d*-electrons of Ti may be responsible for the superconducting behaviour in nanolaminates. One also notes that T_c value is more than doubled when C atoms are replaced by N atoms in the Ti_2InX compound.

3.3. Thermodynamic Properties at Elevated Temperature and Pressure. The elastic parameters and associated physical quantities like Debye temperature, allow a deeper understanding of the relationship between the mechanical properties and the electronic and phonon structure of materials. We investigated the thermodynamic properties of Ti_2InC and Ti_2InN by using the quasiharmonic Debye model, the detailed description of which can be found in literature [30]. For this we need *E-V* data obtained from Birch-Murnaghan third-order EOS [31] using zero temperature and zero pressure equilibrium values, E_0, V_0, and B_0, based on DFT method. Then the thermodynamic properties at finite-temperature and finite-pressure can be obtained using the model. The nonequilibrium Gibbs function $G^*(V; P, T)$ can be written in the form [30]:

$$G^*(V; P, T) = E(V) + PV + A_{\text{vib}}[\Theta(V); T], \quad (1)$$

where $E(V)$ is the total energy per unit cell, PV corresponds to the constant hydrostatic pressure condition, $\Theta(V)$ is the Debye temperature, and A_{vib} is the vibrational term, which can be written using the Debye model of the phonon density of states as [30]:

$$A_{\text{vib}}(\Theta, T) = nkT\left[\frac{9\Theta}{8T} + 3\ln\left(1 - \exp\left(-\frac{\Theta}{T}\right)\right) - D\left(\frac{\Theta}{T}\right)\right], \quad (2)$$

where n is the number of atoms per formula unit, $D(\Theta/T)$ represents the Debye integral.

A minimization of $G^*(V; P, T)$ with respect to volume V can now be made to obtain the thermal equation of state $V(P, T)$ and the chemical potential $G(P, T)$ of the corresponding phase. Other macroscopic properties can also be derived as a function of P and T from standard thermodynamic relations [30]. Here we computed the bulk modulus, Debye temperature specific heats, and volume

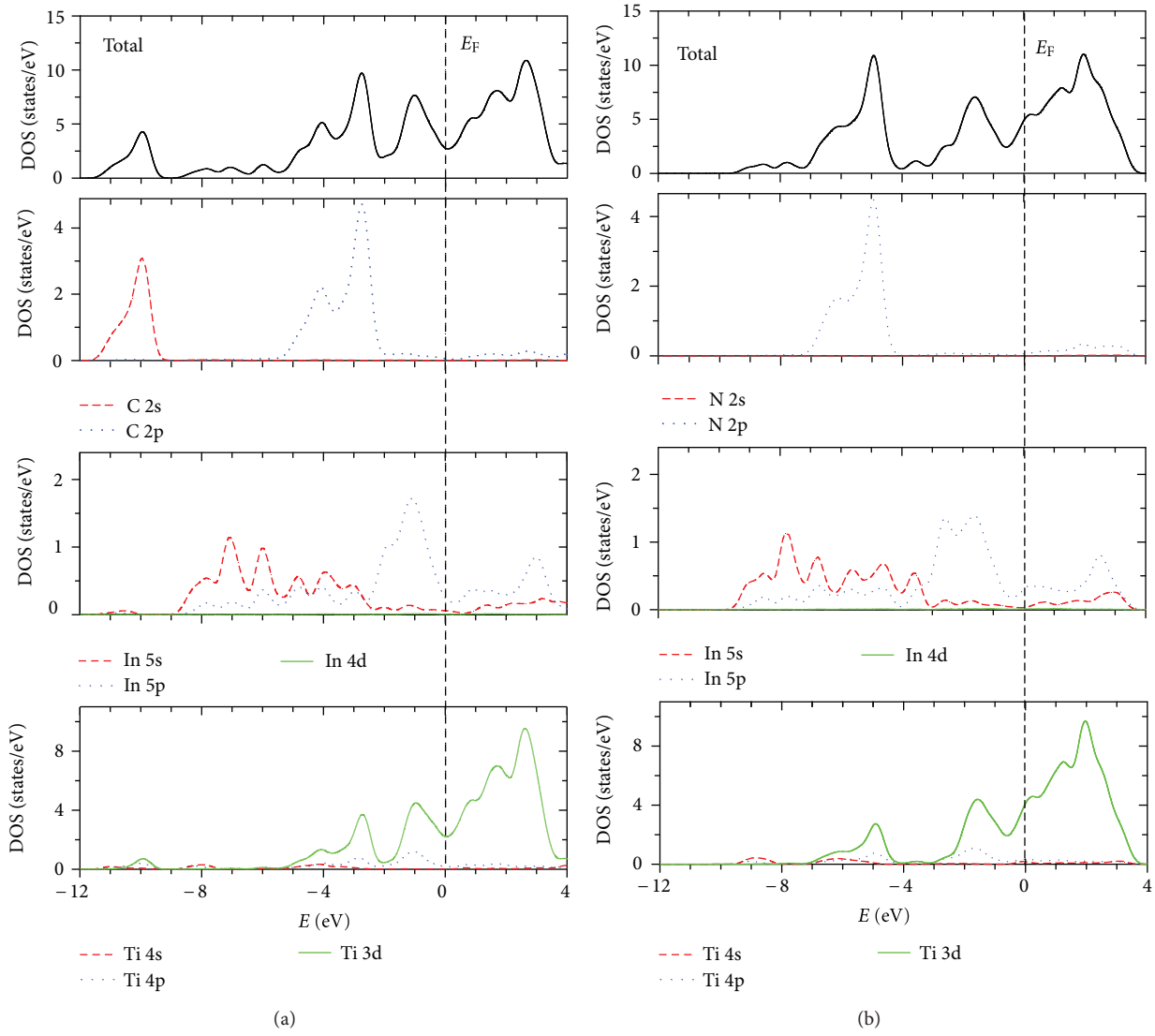

Figure 3: Total and partial DOSs of (a) Ti_2InC and (b) Ti_2InN.

thermal expansion coefficient at different temperatures and pressures.

The temperature variation of isothermal bulk modulus B of Ti_2InC and Ti_2InN is shown in Figure 4(a) and the *inset* of which shows B as a function of pressure. We see that there is hardly any difference in the values of B for the two phases and these vary almost identically as a function of temperature. This means that for the same compressive stress applied to both carbide and nitride phases at a particular temperature results in the same volume strain in both of these. Further the B values, signifying the average strength of the coupling between the neighboring atoms, of 126.4 and 125.5 GPa for Ti_2InC and Ti_2InN, respectively, at 0 K are the smallest among all the superconducting MAX phases [20]. Moreover, it is found that the bulk modulus increases with pressure at a given temperature and decreases with temperature at a given pressure, which is consistent with the trend of volume of the nanolaminates.

Figure 4(b) displays temperature dependence of Debye temperature Θ_D at zero pressure of Ti_2InC and Ti_2InN. One observes that Θ_D, smaller for nitride phase, decrease nonlinearly with temperature for both the phases. Further Θ_D presented as *inset* of Figure 4(b) at $T = 300$ K shows a nonlinear increase. The variation of Θ_D with pressure and temperature reveals that the thermal vibration frequency of atoms in the nanolaminates changes with pressure and temperature. From knowledge of the calculated Debye temperature the value of the electron-phonon coupling constant (λ) can be estimated from McMillan's relation [37]:

$$\lambda = \frac{1.04 + \mu^* \ln\left(\Theta_D/1.45T_c\right)}{\left(1 - 0.62\mu^*\right)\ln\left(\Theta_D/1.45T_c\right) - 1.04}, \quad (3)$$

where μ^* is a Coulomb repulsion constant (typical value, $\mu^* = 0.13$). Utilizing the measured T_c values and the calculated Debye temperatures, we find $\lambda \sim 0.49$ and 0.62, for Ti_2InC

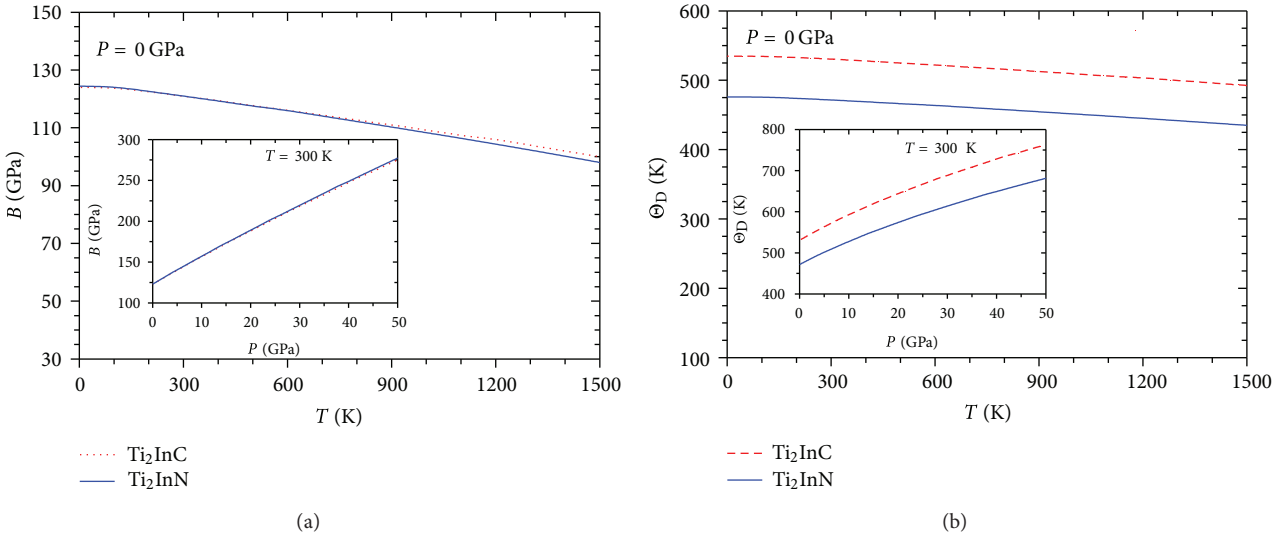

FIGURE 4: Temperature dependence of (a) Bulk modulus and (b) Debye temperature of Ti_2InC and Ti_2InN. *Inset* shows pressure variation.

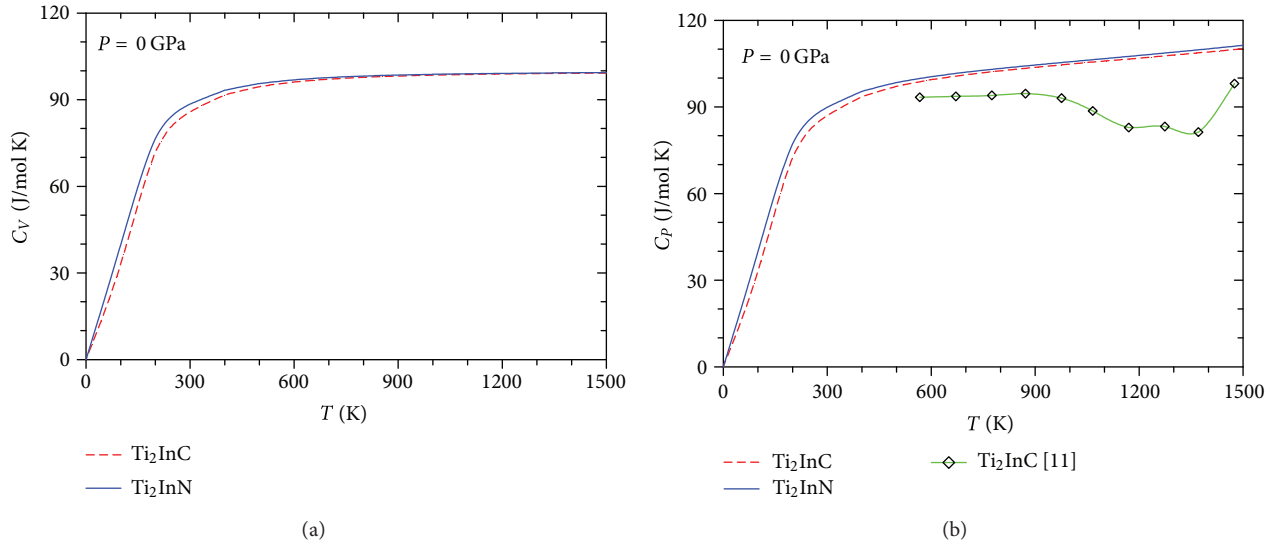

FIGURE 5: Temperature dependence of specific heat at constant (a) volume and (b) pressure of Ti_2InC and Ti_2InN.

and Ti_2InN, respectively. The values imply that both of these are moderately coupled superconductors.

Figures 5(a) and 5(b) show the temperature dependence of constant-volume and constant-pressure specific heat capacities C_V, C_P of Ti_2InC and Ti_2InN. We know that phonon thermal softening occurs when the temperature increases and hence the heat capacities increase with increasing temperature. It should be noted that the heat capacity anomaly close to T_c value (3.1 and 7.3 K, for the two superconductors) is so small (about 0.1%) that it has no effect on the analysis being made here. The only measured C_P data for Ti_2InC due to Barsoum et al. [11] show complex behaviour as shown on the theoretical graph. Even the authors themselves remark that such a complex behaviour is not expected from a single-phase solid that does not go through phase transitions. The drop in C_P must be related to loss of In atoms from the sample. This type of loss would be endothermic and thus exhibits a trough as observed. Barsoum et al. [11] acknowledged that the heat capacity measurements should be repeated with larger samples where the surface to volume ratio is reduced. The increase at higher temperatures is most likely due to oxidation.

The volume thermal expansion coefficient, α_V as a function of both temperature and pressure is displayed in Figure 6. The expansion coefficient is seen to increase rapidly especially at temperature below 300 K, whereas it gradually tends to a slow increase at higher temperatures. On the other hand at a constant temperature, the expansion coefficient decreases strongly with pressure. It is well-known that the thermal expansion coefficient is inversely related to the bulk modulus

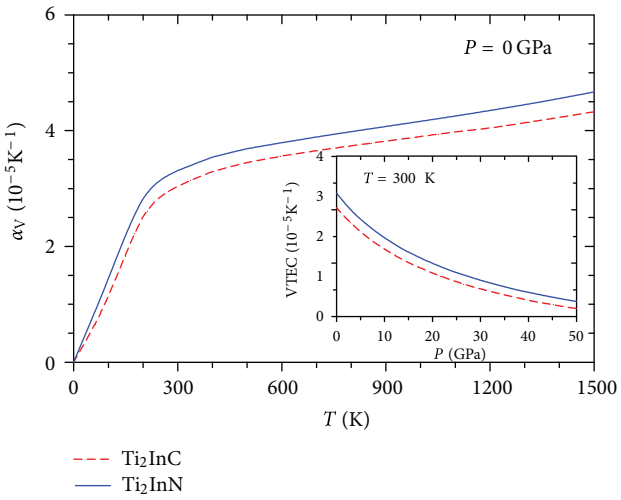

FIGURE 6: Temperature dependent thermal expansion coefficient of Ti_2InC and Ti_2InN. *Inset* shows pressure variation.

of a material. The calculated values of α_V at 300 K for Ti_2InC and Ti_2InN are 3.04×10^{-5} and 3.3×10^{-5} K^{-1}, respectively. The measured value of linear thermal expansion coefficient of Ti_2InC is 9.5×10^{-6} K^{-1} [11]. Assuming, linear thermal expansion coefficient = $\alpha_V/3$, the calculated value of 10.1×10^{-6} K^{-1} for Ti_2InC is in fair agreement with experiment.

3.4. Optical Properties. The study of the optical functions of solids provides a better understanding of the electronic structure. The imaginary part of complex dielectric function, $\varepsilon(\omega) = \varepsilon_1(\omega) + i\varepsilon_2(\omega)$, is obtained from the momentum matrix elements between the occupied and the unoccupied electronic states. This is calculated directly using [38]

$$\varepsilon_2(\omega) = \frac{2e^2\pi}{\Omega\varepsilon_0} \sum_{k,v,c} |\psi_k^c| u \cdot r |\psi_k^v|^2 \delta\left(E_k^c - E_k^v - E\right), \quad (4)$$

where ψ_k^c and ψ_k^v are the conduction and valence band wave functions at k, respectively, u is the vector defining the polarization of the incident electric field, ω is the light frequency, and e is the electronic charge. The Kramers-Kronig transform of the imaginary part $\varepsilon_2(\omega)$ provides the real part. Equations (49) to (54) in [38] define all other optical constants, such as refractive index, absorption spectrum, loss-function, reflectivity, and conductivity (real part).

The calculated optical functions of Ti_2InC and Ti_2InN for photon energies up to 20 eV for polarization vectors [100] and [001] (only spectra for [100] shown) along with measured spectra of TiC and TiN (where available) are shown in Figure 7. We have used a 0.5 eV Gaussian smearing for all calculations. The calculations only include interband exciatations. In metal and metal-like systems there are intraband contributions from the conduction electrons mainly in the low-energy infrared part of the spectra. It is thus necessary to include this via an empirical Drude term to the dielectric function [39, 40]. A Drude term with plasma frequency 3 eV and damping (relaxation energy) 0.05 eV was used.

Despite some variation in heights and positions of peaks, the overall features of our calculated optical spectra of Ti_2InC and Ti_2InN are roughly similar. In the energy range for which $\varepsilon_1(\omega) < 0$, Ti_2InC, and Ti_2InN exhibit the metallic characteristics (Figure 7(a)). The result of Ti_2InC is somewhat different as regards the energy range for negativity of $\varepsilon_1(\omega)$. The dielectric function of Ti_2InC is compared with that of $TiC_{0.9}$ [33]. We see that the double peak structure centred at 1.7 eV for $TiC_{0.9}$ is replaced with a sharp peak at around 0.7 eV for Ti_2InC. The spectra differ at low energy due to the electronic structure change near the Fermi level, induced by the addition of In layer in TiC. The same inference can be made when one compares low-energy spectra of Ti_2InN and TiN [34]. On the other hand no maxima are seen in ε_2 for the two MAX phases, although the values are large in the low-energy region (Figure 7(b)). The corresponding spectra for $TiC_{0.9}$ [33] and TiN [34] are shown for comparison. The refractive index and extinction coefficients of the nanolaminates are displayed in Figures 7(c) and 7(d).

The absorption coefficient provides data about optimum solar energy conversion efficiency and it indicates how far light of a specific energy (wavelength) can penetrate into the material before being absorbed. Figure 7(e) shows the absorption coefficients of both the phases which begin at 0 eV due to their metallic nature. Ti_2InC has two peaks, one at ~4.3 eV (same for Ti_2InN) and the other at 6.3 eV (8 eV for Ti_2InN), besides having a shoulder at lower energy. Both the nanolaminates show rather good absorption coefficient in the 4–10 eV region. The energy loss $L(\omega)$ of a fast electron traversing in the material is depicted in Figure 7(f). The bulk plasma frequency ω_P is at the peak position which occurs at $\varepsilon_2 < 1$ and $\varepsilon_1 = 0$. In the energy-loss spectrum, we see that ω_P of the two phases Ti_2InC and Ti_2InN are ~13.2 eV and ~12.8 eV, respectively. When the incident photon frequency is higher than ω_P, the material becomes transparent.

Figure 7(g) presents the reflectivity spectra as a function of photon energy in comparison with measured spectra of $TiC_{0.97}$ [33] and TiN [35]. The reflectance for $TiC_{0.97}$ is nearly constant over the energy range considered. With addition of In to TiC the reflectivity is much higher in the infrared region, it then decreases sharply to 0.55 which becomes almost steady till 5 eV. After an increase with photon energy up to ~10 eV, the reflectivity falls again. On the other hand we find that the reflectivity in Ti_2InN is high in IR-visible-UV up to ~ 12.8 eV region (reaching maximum between 10 and 12.8 eV). Compared to this the reflectivity of TiN starts with a higher value in the infrared and there is a sharp drop between 2 and 3 eV, which is the characteristics of high conductance [35]. The low reflectivity in the region of visible blue and violet light (2.8–3.5 eV) increases to a value of 0.36 at 6 eV (ultraviolet). The analysis shows that the nitride phase would be a comparatively better material as promising candidate for use as coating material.

Figure 7(h) shows that the photoconductivity starts with zero photon energy due to the reason that the materials have no band gap which is evident from band structure. Moreover, the photoconductivity and hence electrical conductivity of a material increases as a result of absorbing photons.

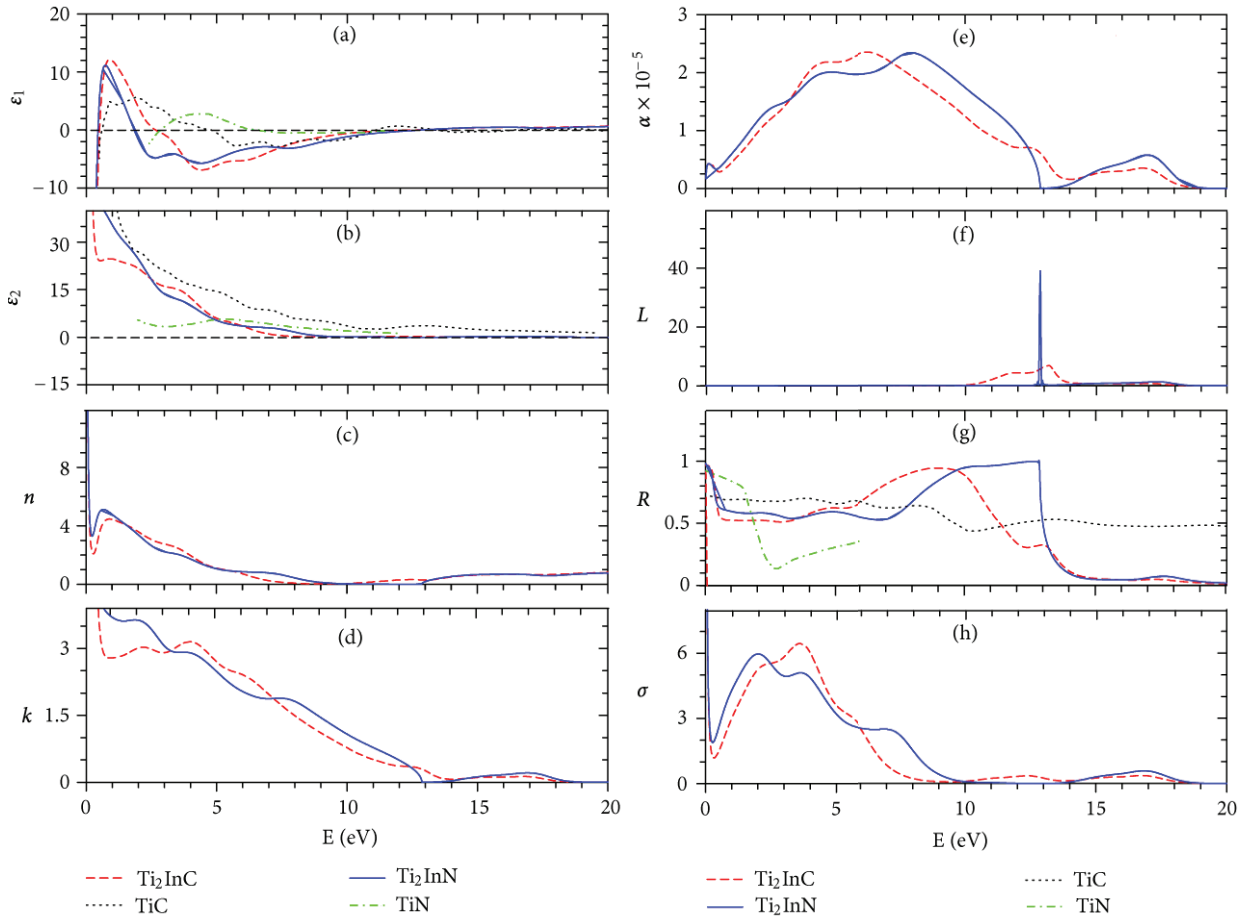

FIGURE 7: Energy dependent (a) real part of dielectric function, (b) imaginary part of dielectric function, (c) refractive index, (d) extinction coefficient, (e) absorption, (f) loss function, (g) reflectivity, and (h) real part of conductivity of Ti_2InC and Ti_2InN along [100] direction. Experimental data shown for TiC and TiN are from [33–35], respectively.

4. Conclusion

We have performed a first-principles calculations based on DFT to compare the structural, elastic, thermodynamic, electronic, and optical properties of the two superconducting MAX phases Ti_2InC and Ti_2InN. The obtained elastic constants are compared with available calculations and elastic anisotropy discussed. The carbide phase is found to be brittle in nature, while the nitride phase is less brittle (near the border line).

The energy band structure and total densities of states reveal that both the materials exhibit metallic conductivity. This conductivity increases as X is changed from C atom to N in Ti_2InX. Hybridization of Ti-atom d states with C (N)-atom p states is responsible for the bonding. The Ti–In bond is weaker and the order of the bond strength: Ti–N > Ti–C > Ti–In. The bands associated with N atoms are lower in energy and narrower that can be attributed to the large electronegativity of N compared to that of C.

The temperature and pressure dependence of bulk modulus, specific heats, thermal expansion coefficient, and Debye temperature are all obtained through the quasiharmonic Debye model, and the results are analyzed. We find the electron-phonon coupling strengths $\lambda \sim 0.49$ and 0.62 for Ti_2InC and Ti_2InN, respectively, which implies that both are moderately coupled superconductors. The heat capacities increase with increasing temperature, which shows that phonon thermal softening occurs when the temperature increases. The thermal expansion coefficients for Ti_2InC and Ti_2InN are evaluated, and the calculation is in fair agreement with the only measured value available for Ti_2InC.

The optical features such as the real and imaginary parts of the dielectric function and positive dielectric constant do show to support the potential applications of the compounds in future. The reflectivity is high in the IR-visible-UV region up to ~10 eV and 12.8 eV for Ti_2InC and Ti_2InN, respectively, showing promise as good coating materials.

References

[1] H. Nowotny, *Progress in Solid State Chemistry*, vol. 2, Pergamon Press, New York, NY, USA, 1970, edited by H. Reiss.

[2] M. W. Barsoum, "$M_{N+1}AX_N$ phases: a new class of solids; thermodynamically stable nanolaminates," *Progress in Solid State Chemistry*, vol. 28, no. 1–4, pp. 201–281, 2000.

[3] P. Eklund, M. Beckers, U. Jansson, H. Högberg, and L. Hultman, "The $M_{n+1}AX_n$ phases: materials science and thin-film processing," *Thin Solid Films*, vol. 518, no. 8, pp. 1851–1878, 2010.

[4] L. E. Toth, "High superconducting transition temperatures in the molybdenum carbide family of compounds," *Journal of The Less-Common Metals*, vol. 13, no. 1, pp. 129–131, 1967.

[5] K. Sakamaki, H. Wada, H. Nozaki, Y. Onuki, and M. Kawai, "Carbosulfide superconductor," *Solid State Communications*, vol. 112, no. 6, pp. 323–327, 1999.

[6] A. D. Bortolozo, O. H. Sant'Anna, M. S. da Luz et al., "Superconductivity in the Nb_2SnC compound," *Solid State Communications*, vol. 139, no. 2, pp. 57–59, 2006.

[7] S. E. Lofland, J. D. Hettinger, T. Meehan et al., "Electron-phonon coupling in $M_{n+1}AX_n$-phase carbides," *Physical Review B*, vol. 74, no. 17, Article ID 174501, 5 pages, 2006.

[8] A. D. Bortolozo, O. H. Sant'Anna, C. A. M. dos Santos, and A. J. S. Machado, "Superconductivity in the hexagonal-layered nanolaminates Ti_2InC compound," *Solid State Communications*, vol. 144, no. 10-11, pp. 419–421, 2007.

[9] A. D. Bortolozo, Z. Fisk, O. H. Sant'Anna, C. A. M. dos Santos, and A. J. S. Machado, "Superconductivity in Nb_2InC," *Physica C*, vol. 469, no. 7-8, pp. 256–258, 2009.

[10] A. D. Bortolozo, G. Serrano, A. Serquis et al., "Superconductivity at 7.3 K in Ti_2InN," *Solid State Communications*, vol. 150, no. 29-30, pp. 1364–1366, 2010.

[11] M. W. Barsoum, J. Golczewski, H. J. Seifert, and F. Aldinger, "Fabrication and electrical and thermal properties of Ti_2InC, Hf_2InC and $(Ti,Hf)_2InC$," *Journal of Alloys and Compounds*, vol. 340, no. 1-2, pp. 173–179, 2002.

[12] W. Jeitschko, H. Nowotny, and F. Benesovsky, "Die H-phasen Ti_2InC, Zr_2InC, Hf_2InC und Ti_2GeC," *Monatshefte für Chemie*, vol. 94, no. 6, pp. 1201–1205, 1963.

[13] W. Jeitschko, H. Nowotny, and F. Benesovsky, "Die H-phasen: Ti_2CdC, Ti_2GaC, Ti_2GaN, Ti_2InN, Zr_2InN und Nb_2GaC," *Monatshefte für Chemie*, vol. 95, no. 1, pp. 178–179, 1964.

[14] B. Manoun, O. D. Leaffer, S. Gupta et al., "On the compression behavior of Ti_2InC, $(Ti_{0.5}, Zr_{0.5})_2InC$, and M_2SnC (M = Ti, Nb, Hf) to quasi-hydrostatic pressures up to 50 GPa," *Solid State Communications*, vol. 149, no. 43-44, pp. 1978–1983, 2009.

[15] I. R. Shein and A. L. Ivanovskiĭ, "Electronic and elastic properties of the superconducting nanolaminate Ti_2InC," *Physics of the Solid State*, vol. 51, no. 8, pp. 1608–1612, 2009.

[16] A. L. Ivanovskii, R. F. Sabiryanov, A. N. Skazkin, V. M. Zhukovskii, and G. P. Shveikin, "Electronic structure and bonding configuration of the *H*-phases Ti_2MC and Ti_2MN (M = Al, Ga, In)," *Inorganic Materials*, vol. 36, no. 1, pp. 28–31, 2000.

[17] G. Hug, "Electronic structures of and composition gaps among the ternary carbides Ti_2MC," *Physical Review B*, vol. 74, no. 18, Article ID 184113, 7 pages, 2006.

[18] Y. Medkour, A. Bouhemadou, and A. Roumili, "Structural and electronic properties of M_2InC (M = Ti, Zr, and Hf)," *Solid State Communications*, vol. 148, no. 9-10, pp. 459–463, 2008.

[19] X. He, Y. Bai, Y. Li, C. Zhu, and M. Li, "*Ab initio* calculations for properties of MAX phases Ti_2InC, Zr_2InC, and Hf_2InC," *Solid State Communications*, vol. 149, no. 13-14, pp. 564–566, 2009.

[20] I. R. Shein and A. L. Ivanovskii, "Elastic properties of superconducting MAX phases from first-principles calculations," *Physica Status Solidi B*, vol. 248, no. 1, pp. 228–232, 2011.

[21] O. D. Leaffer, S. Gupta, M. W. Barsoum, and J. E. Spanier, "On Raman scattering from selected M_2AC compounds," *Journal of Materials Research*, vol. 22, no. 10, pp. 2651–2654, 2007.

[22] N. Benayad, D. Rached, R. Khenata et al., "First principles study of the structural, elastic and electronic properties of Ti_2InC and Ti_2InN," *Modern Physics Letters B*, vol. 25, no. 10, pp. 747–761, 2011.

[23] B. Liu, J. Y. Wang, J. Zhang, J. M. Wang, F. Z. Li, and Y. C. Zhou, "Theoretical investigation of *A*-element atom diffusion in Ti_2AC (A = Sn, Ga, Cd, In, and Pb)," *Applied Physics Letters*, vol. 94, no. 18, Article ID 181906, 3 pages, 2009.

[24] J. Haines, J. M. Léger, and G. Bocquillon, "Synthesis and design of superhard materials," *Annual Review of Materials Science*, vol. 31, pp. 1–23, 2001.

[25] W. Kohn and L. Sham, "Self-consistent equations including exchange and correlation effects," *Physical Review*, vol. 140, no. 4, pp. A1133–A1138, 1965.

[26] S. J. Clark, M. D. Segall, C. J. Pickard et al., "First principles methods using CASTEP," *Zeitschrift fur Kristallographie*, vol. 220, no. 5-6, pp. 567–570, 2005.

[27] J. P. Perdew, K. Burke, and M. Ernzerhof, "Generalized gradient approximation made simple," *Physical Review Letters*, vol. 77, no. 18, pp. 3865–3868, 1996.

[28] H. J. Monkhorst and J. D. Pack, "Special points for Brillouin-zone integrations," *Physical Review B*, vol. 13, no. 12, pp. 5188–5192, 1976.

[29] T. H. Fischer and J. Almlöf, "General methods for geometry and wave function optimization," *Journal of Physical Chemistry*, vol. 96, no. 24, pp. 9768–9774, 1992.

[30] M. A. Blanco, E. Francisco, and V. Luaña, "GIBBS: Isothermal-isobaric thermodynamics of solids from energy curves using a quasi-harmonic Debye model," *Computer Physics Communications*, vol. 158, no. 1, pp. 57–72, 2004.

[31] F. Birch, "Finite strain isotherm and velocities for single-crystal and polycrystalline NaCl at high pressures and 3000 K," *Journal of Geophysics Research*, vol. 83, no. B3, p. 1257, 1978.

[32] M. W. Barsoum, "Physical properties of MAX phases," in *Encyclopedia of Materials: Science and Technology*, p. 1, Elsevier, Amsterdam, The Netherlands, 2006.

[33] D. W. Lynch, C. G. Olson, D. J. Peterman, and J. H. Weaver, "Optical properties of TiC_x ($0.64 \leq x \leq 0.90$) from 0.1 to 30 eV," *Physical Review B*, vol. 22, no. 8, pp. 3991–3997, 1980.

[34] R. Eibler, M. Dorrer, and A. Neckel, "Calculation of the imaginary part $\epsilon_2(\omega)$ of the dielectric function for TiN and ZrN," *Journal of Physics C*, vol. 16, no. 16, pp. 3137–3148, 1983.

[35] B. Karlsson, *Optical properties of solids for solar energy conversion [Ph.D. thesis]*, Acta Universitatis Upsaliensis, Uppsala, Sweden, 1981.

[36] N. I. Medvedeva, A. N. Enyashin, and A. L. Ivanovskii, "Modeling of the electronic structure, chemical bonding, and properties of ternary silicon carbide Ti_3SiC_2," *Journal of Structural Chemistry*, vol. 52, no. 4, pp. 785–802, 2011.

[37] W. L. McMillan, "Transition temperature of strong-coupled superconductors," *Physical Review*, vol. 167, no. 2, pp. 331–344, 1968.

[38] Materials Studio CASTEP Manual Accelrys, 2010, http://www.tcm.phy.cam.ac.uk/castep/documentation/WebHelp/CASTEP.html.

[39] S. Li, R. Ahuja, M. W. Barsoum, P. Jena, and B. Johansson, "Optical properties of Ti_3SiC_2 and Ti_4AlN_3," *Applied Physics Letters*, vol. 92, no. 22, Article ID 221907, 3 pages, 2008.

[40] R. Saniz, L. H. Ye, T. Shishidou, and A. J. Freeman, "Structural, electronic, and optical properties of $NiAl_3$: first-principles calculations," *Physical Review B*, vol. 74, no. 1, Article ID 014209, 7 pages, 2006.